International Journal of Biometeorology (2021) 65:905–915
https://doi.org/10.1007/s00484-020-02072-y

ORIGINAL PAPER

# A July-August relative humidity record in North China since 1765 AD reconstructed from tree-ring cellulose $\delta^{18}O$

Linlin Cui[1,2] · Yu Liu[1,3,4,5] · Qiang Li[1] · Huiming Song[1] · Congxi Fang[1]

Received: 28 July 2020 / Revised: 16 December 2020 / Accepted: 23 December 2020 / Published online: 2 February 2021


**Abstract**
Since the late 1970s, East Asian summer monsoon (EASM) has shown a significant weakening trend, and sustained drought has occurred across North China. Placing recent climate changes in the paleoclimatic context can better understand the EASM variations. Four $\delta^{18}O$ sequences based on tree-ring cellulose of Chinese pine were developed from Mt. Beiwudang, North China, covering a period from 1700 to 2013. Based on a climatic response analysis, a transfer function was designed to reconstruct the relative humidity from July to August ($RH_{JA}$ hereafter). The $RH_{JA}$ spans from 1765 to 2013 and explains 49% ($R^2_{adj} = 48\%$) of the instrumental variance during the calibration period (1961–2013, $r = -0.70$, $p < 0.0001$). The $RH_{JA}$ is mainly influenced by precipitation in the summer rainy season and reflect EASM variations. Spatial representation analysis indicates that $RH_{JA}$ represents the dry/wet variations across North China. At the interannual scale, $RH_{JA}$ records many extreme dry/wet events, among which the events in 1876–1878, 1900, and the 1920s are extensive droughts. Those events correspond well to ENSO events, plus further correlation and periodicity analysis indicate that $RH_{JA}$ contains ENSO signals. At the interdecadal scale, $RH_{JA}$ shows a decreasing trend and unprecedented low values from 1981 to 2013, suggesting that the weakening of EASM since the late 1970s is unprecedented in the past 249 years. Similarly, the significantly correlating region in the spatial correlation analysis, covering the Meiyu/Baiu/Changma rainfall belt and India, have also undergone a climatic shift since the late 1970s according to previous papers.

**Keywords** Tree-ring cellulose · $\delta^{18}O$ · Climatic variations · North China · Drought events · Eastern Asian summer monsoon

## Introduction

Summer monsoon precipitation is very important to agricultural and social development in monsoon regions, and drought and flood disasters caused by abnormal changes of the monsoon affect the socioeconomic status of the people living in these regions, which accounts for two-thirds of the world's population. To better adapt to the complex and fluctuating natural environment in monsoon areas, it is necessary to understand the temporal and spatial variations of monsoon precipitation. However, although precipitation in the monsoon area is mainly controlled by monsoons (An et al. 2000), spatial divergence of monsoon precipitation exists in the East Asian summer monsoon (EASM) region (Ding et al. 2008; Zhou et al. 2009a). Therefore, it is necessary to investigate the history of hydrological climate change in North China.

Considering the time span, it is often not enough to understand past climate change using only instrumental data. Using paleoclimatic data to place recent climate changes in the context of centuries or millennia is helpful for grasping the climatic variation pattern and then predicting future climate change (Ljungqvist et al. 2016). Tree rings are one of the most ideal proxy materials for recording climate change over the past century and millennium because of their dating accuracy,

✉ Yu Liu
liuyu@loess.llqg.ac.cn

1 The State Key Laboratory of Loess and Quaternary Geology, Institute of Earth Environment, Chinese Academy of Sciences, Xi'an 710061, China

2 The University of the Chinese Academy of Sciences, Beijing 100049, China

3 Center for Excellence in Quaternary Science and Global Change, Chinese Academy of Sciences, Xi'an 710061, China

4 Qingdao National Laboratory for Marine Science and Technology, Qingdao 266237, China

5 School of Human Settlements and Civil Engineering, Xi'an Jiaotong University, Xi'an 710049, China

temporal continuity, temporal resolution (annual and even seasonal resolution), and wide geographical distribution. Climatic information of the past century or even millennium (Yang et al. 2014) has been obtained from tree rings, covering most parts of the world (Mann et al. 2009). Cai et al. (2010) reconstructed the average temperature from May to July based on tree-ring widths of Chinese pine on Mt. Beiwudang. However, besides traditional tree-ring width, many other research methods have been developed in dendroclimatology (Pearl et al. 2020), such as tree-ring density (Briffa et al. 2001), stable isotope ratio (McCarroll and Loader 2004), and wood anatomy (Fonti et al. 2010). Due to its clear physiological mechanism and the ability to maintain low-frequency climatic signals, tree-ring stable isotope climatic reconstruction has developed rapidly in the past few decades (McCarroll and Loader, 2004). Furthermore, because many tree-ring $\delta^{18}O$ reconstruction results around the study area have shown significant correlations with hydroclimatic parameters (Li et al. 2011; Liu et al. 2020), we established a tree-ring $\delta^{18}O$ record of Mt. Beiwudang to investigate the hydroclimatic variations in adjacent regions.

## Materials and methods

### Study area and field sampling

The sampling site is located on Mt. Beiwudang (37° 46′ N, 111° 20′ E, 1740–1900 m above sea level, Fig. 1a), situated in North China and belonging to the East Asian Monsoon Region (Ding and Chan 2005). This mountainous area is far from cities, where the dominant coniferous tree species is Chinese pine (*Pinus tabulaeformis* Carr.), growing with little human disturbance. The sampling strategy follows dendroclimatological practices (Fritts 1976; Leavitt 2010), targeting climatic-sensitive trees growing on steep rock slopes with a thin soil layer, with discontinuous canopies and no pests or diseases. To facilitate cross-dating, 19 Chinese pines of different ages were sampled using a 10-mm-diameter increment borer at breast height (two cores per tree).

### Climatic data

In consideration of the large spatial representativeness of tree-ring oxygen isotope proxy data (Liu et al. 2020), three national meteorological stations, i.e., Yan'an (36° 36′ N, 109° 30′ E), Taigu (37° 26′ N, 112° 32′ E), and Xingxian (38° 28′ N, 111° 08′ E), were selected to determine the climatic variations across the studied region. They are evenly distributed in different directions near the sampling site (Fig. 1a). The instrumental data were obtained from the China Meteorological Science Data Sharing Service Network (http://data.cma.cn/). From 1961 to 2013 AD, there were no records of relocation or monthly data missing from the three meteorological stations, and data variations conformed to a normal distribution. The similar monthly distribution of climatic data (averaged over 1961–2013 AD) suggests that the three meteorological stations are located in the same climate area with a temperate continental monsoon climate (Fig. 1b). Therefore, the arithmetic average of the instrumental data from the three stations can be used to represent the regional climatic variation.

There are many climate indices used in this study, where the East Asian Summer Monsoon Index (EASMI) has different definitions. The EASMI (Shi and Zhu 1996) is defined as the sum of the standardized sea-level air pressure (SLP) differences (110° E minus 160° E) at seven parallels between 20° N and 50° N, and then the sum is standardized again. Because there is low pressure over the Asian continent and a subtropical high over the ocean in summer, a more negative EASMI denotes a stronger monsoon flow. The EASMI (Lau et al. 2000) is defined as a shear vorticity index of 200-hPa zonal winds, mainly focusing on the upper-tropospheric westerly jet stream. The EASMI (Huang and Yan 1999) reflects 500-hPa vorticity at three grids in the East Asia-Pacific (EAP) region, focusing on the EAP teleconnection. NINO1+2, NINO3, NINO3.4, and NINO4 are sea surface temperature anomalies in the NINO1+2 region (80° W–90° W, 0°–20° S), NINO3 region (90° W–150° W, 20° S–20° N), NINO3.4 region (120° W–170° W, 20° S–20° N), and NINO4 region (150° E–160° W, 20° S–20° N), respectively, based on the ERSST v5 dataset. The SOI is the Southern Oscillation Index from standardized NCEP Tahiti-Darwin SLP data, historical data, and recent data (http://www.cpc.ncep.noaa.gov/data/indices/soi). The MEI is the Multivariate ENSO Index (http://www.cdc.noaa.gov/people/klaus.wolter/MEI/ESRL).

### The developing of tree-ring cellulose $\delta^{18}O$ sequences

The tree-ring cellulose $\delta^{18}O$ sequences were developed after following experimental steps.

**Cross-dating** The tree-ring widths were measured by a Lintab Tree-ring Width Measurement System at a resolution of 0.01

**Fig. 1** **a** Map showing the locations of the sampling site in this study (Mt. Beiwudang, green triangle), meteorological stations (black circles), comparison sites from previous studies (yellow block and box), and the regional instrumental data covering the Meiyu/Baiu/Changma rainfall belt (blue box). Spatial correlation analysis result of the $RH_{JA}$ based on the CRU TS 4.04 (land) precipitation dataset during July-August from 1961 to 2013 AD is shown in the map, and only the significantly correlating region ($p < 10\%$) is colored, where red denotes positive and blue denotes negative. **b** Monthly distribution of precipitation, temperature, and relative humidity for three meteorological stations during 1961–2013. **c** The reconstructed $RH_{JA}$, regional observed rainfall of the blue box shown in Fig. 1a and their 21-year moving correlation, where the arrow denotes the recent rainfall trend

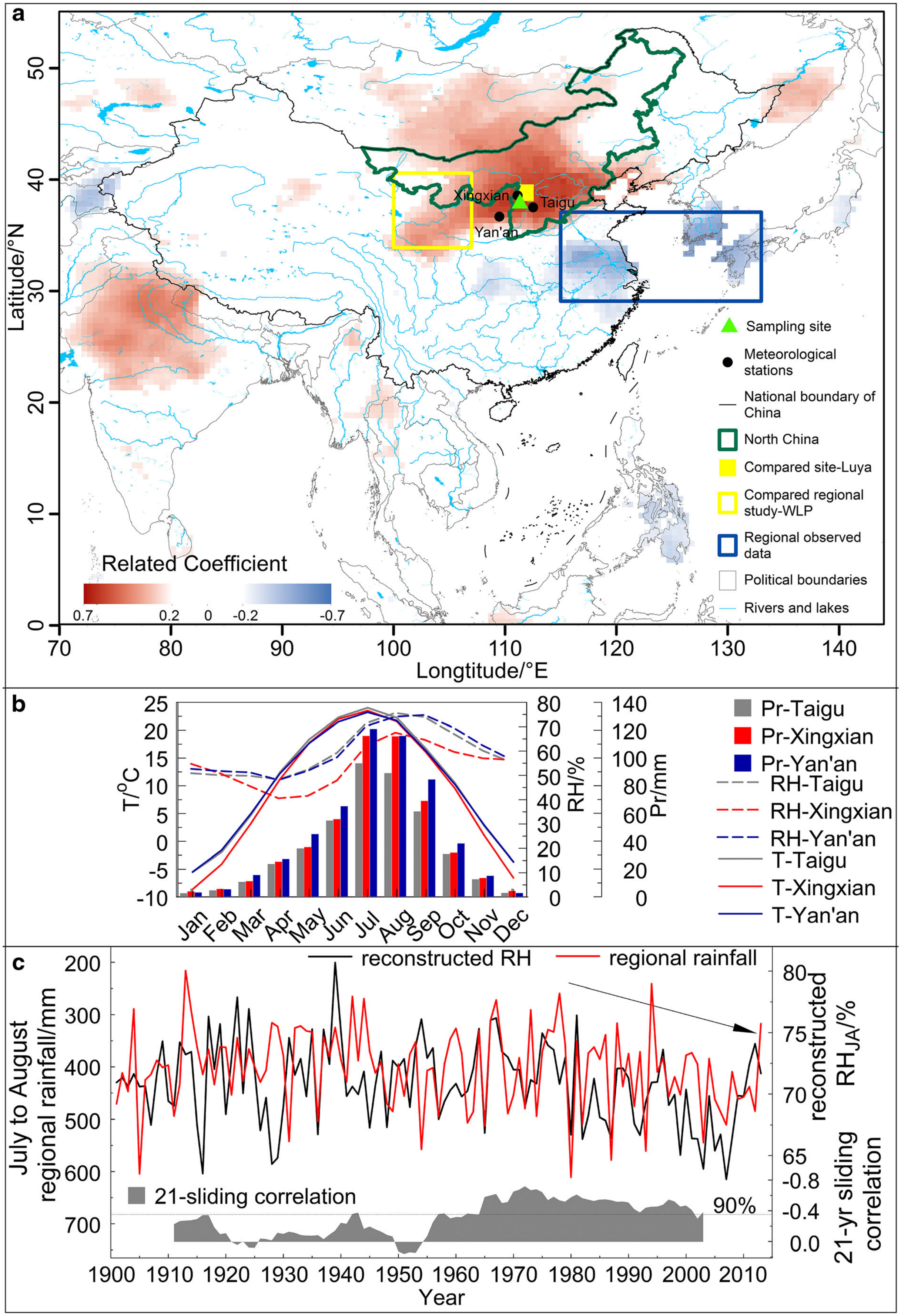
a
Latitude/°N
Longtitude/°E
Xingxian
Taigu
Yan'an
Related Coefficient
0.7 0.2 0 -0.2 -0.7
Sampling site
Meteorological stations
National boundary of China
North China
Compared site-Luya
Compared regional study-WLP
Regional observed data
Political boundaries
Rivers and lakes
b
T/°C
RH/%
Pr/mm
Pr-Taigu
Pr-Xingxian
Pr-Yan'an
RH-Taigu
RH-Xingxian
RH-Yan'an
T-Taigu
T-Xingxian
T-Yan'an
Jan Feb Mar Apr May Jun Jul Aug Sep Oct Nov Dec
c
reconstructed RH
regional rainfall
July to August regional rainfall/mm
reconstructed RHJA/%
21-yr sliding correlation
21-sliding correlation
90%
Year

mm. The calendar year of each ring was confirmed by matching all tree-ring width sequences and then dating according to the sampling time. The quality of cross-dating was controlled by the COFECHA program (Holmes 1983).

**Splitting samples** Four cores with clear ring boundaries and few missing rings were selected for the isotope study. Each ring was split into small pieces (thickness < 0.5 mm) using a razor blade under a microscope and loaded into clean glass bottles marked with the year and core identifier.

**Extracting α-cellulose** The $\alpha$-cellulose was extracted from the samples using a modified Jayme-Wise method (Loader et al. 1997): (i) removed organic impurities using a mixture of methylbenzene and anhydrous alcohol; (ii) decomposed the lignin using acidified $NaClO_2$; (iii) removed hemicellulose using NaOH solution; (iv) homogenized cellulose using an ultrasonic cell disruptor and dried samples using a vacuum freeze-dryer.

**Measuring δ18O values** Each $\alpha$-cellulose sample was packed in a silver capsule and measured automatically one by one. After every 8 samples, a laboratory-standard sample (Merck) was measured to calibrate the measurement results. The Merck sample was a thin-layer cellulose microcrystalline (EMD Millipore Corporation) standard, and its $\delta^{18}$O value (27.70‰VSMOW) was measured with IAEA-601 (Coplen et al. 2006) as a reference. IAEA-601 (benzoic acid) is a reference material recommended by the International Atomic Energy Agency (IAEA). The $\delta^{18}$O values of the samples were measured using a temperature conversion elemental analyzer (TC/EA) interfaced with a Delta V Advantage Isotope Ratio Mass Spectrometer. The analytical precision of the $\delta^{18}$O values of the laboratory-standard samples in this study was ± 0.19‰ VSMOW at a 95% confidence level. Finally, the measured $\delta^{18}O_{tree}$ value was calibrated in reference to Merck samples.

## The compositing of $\delta^{18}O_{tree}$ chronology

In this study, the early period of the result shows low cohesiveness. This is mainly because of the dating error due to low sample depth in the early years. A threshold of expressed population signal (EPS) above 0.85 was selected as a cut-off to delete these years. It is worth noting that the EPS threshold of 0.85 is prevalent but not compulsory for tree-ring climatic studies (Baker et al. 2008; Fowler et al. 2004; Chen et al. 2015). The interval from 1700 to 1764 was ignored due to low cohesiveness (EPS < 0.85) and no duplications (less than 2 cores), and the data from 1765 to 2013 were used to develop the $\delta^{18}O_{tree}$ chronology using a "numerical mix method" (Liu et al. 2012): The $\delta^{18}O_{tree}$ chronology is composited from the arithmetic average of four normalized sequences.

# Results

## $\delta^{18}O_{tree}$ sequences and composite chronology

Four $\delta^{18}O_{tree}$ sequences and the composite chronology were finally obtained (Fig. 2a). EPS is above 0.85 for most of the period (Fig. 2a), suggesting that these four cores are sufficient for tree-ring isotope studies at this site (Wigley et al. 1984; Leavitt 2010). The statistical characteristics of the individual $\delta^{18}O_{tree}$ series and the correlation coefficients among them are shown in Table 1.

## Climatic response

A correlation analysis (Fig. 2b) was conducted between the instrumental data and $\delta^{18}O_{tree}$ chronology during the overlapping period (1961–2013 AD). The $\delta^{18}O_{tree}$ chronology negatively correlated with precipitation in most months, positively correlated with temperature in all months and significantly negatively correlated with relative humidity in April and July-September ($p < 0.05$). Among all monthly combinations, the correlation between $\delta^{18}O_{tree}$ chronology and relative humidity in July-August was the highest ($r = -0.70$, $n = 53$, $p < 0.05$), suggesting that the $\delta^{18}O_{tree}$ chronology for this study area mainly reflects the relative humidity signals from July to August.

## July-August relative humidity reconstruction for Mt. Beiwudang

Based on the climatic response analysis, the relative humidity from July to August was selected for reconstruction. The $\delta^{18}O_{tree}$ chronology and calibration data (relative humidity of July to August for 1961–2013) scatter plot presents a linear distribution (Fig. 2c); hence, we selected a simple linear regression model to design the transfer function as follows:

$$RH_{JA} = 70.81 - 3.97 \times \delta^{18}O_{tree}$$
$$\left(n = 53; r = 0.702; R^2 = 0.49; R^2_{adj} = 0.48; F = 49.58, p < 0.0001; D/W = 2.09\right)$$

where $\delta^{18}O_{tree}$ is the composite chronology of tree-ring cellulose stable oxygen isotope and $RH_{JA}$ is the reconstructed relative humidity from July to August (Fig. 2d). The $RH_{JA}$ explains 49% ($R^2$) of the instrumental variance during the period of 1961–2013, and it reduces to 48% considering the loss of freedom ($R^2_{adj}$). An $F$-test ($F = 49.58$) with a confidence level of $p < 0.0001$ indicates that the linear relationship between the $\delta^{18}O_{tree}$ chronology and observed data is significant. A Durbin-Watson test (Durbin and Watson 1950) suggests that the residual of the reconstruction does not have significant autocorrelation. As shown in Fig. 2e, the $RH_{JA}$ have similar

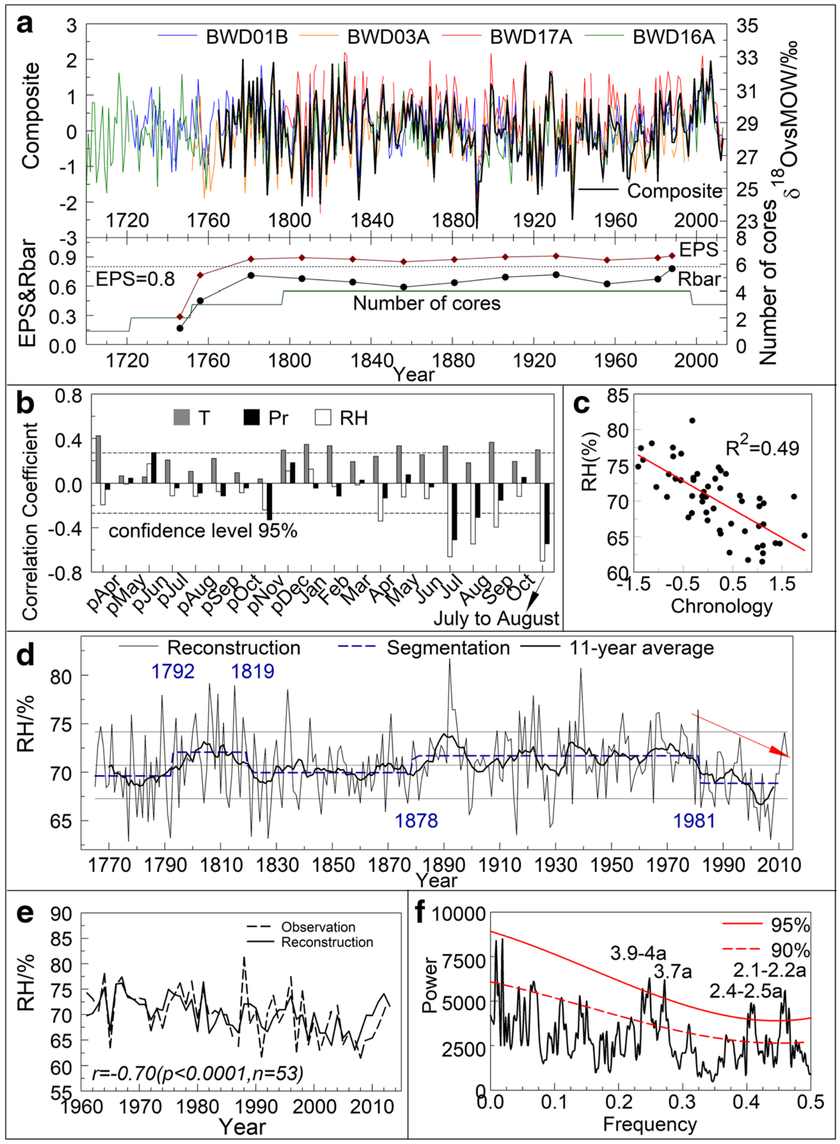


**Fig. 2** **a** $\delta^{18}O_{tree}$ chronology (thick line) and four $\delta^{18}O_{tree}$ sequences (thin line) from Mt. Beiwudang, EPS, Rbar (mean of the correlation coefficients among the samples) and the number of cores, where Rbar and EPS were calculated for every 50 years with a lag of 25 years. **b** Correlation coefficients between instrumental data and $\delta^{18}O_{tree}$ chronology during the overlapping period (1961–2013), where pApr represents the previous-year April for example. **c** The $\delta^{18}O_{tree}$ and calibration data (observed Relative Humidity of July to August for 1961–2013) scatter plot. **d** $RH_{JA}$ during 1765–2013, where the blue dotted line is the average value of each relative dry/wet period, the blue number denotes the shift year of each period, and the arrow indicates the drought trend after the 1970s. **e** The observed data and $RH_{JA}$. **f** Multi-taper method (MTM) spectral analysis

variability with the instrumental data during 1961–2013, and the correlation coefficient ($r$) is − 0.70 ($n$ = 53). In addition, the correlation coefficient of the first-order difference series between the $RH_{JA}$ and instrumental data is − 0.67 ($n$ = 52), which indicates that the correlation between $RH_{JA}$ and instrumental data does not simply trend similarity.

The stability and reliability of the transfer function were tested using the split calibration-verification model (Cook et al. 1999; Fritts 1991). The results of sign test and t test of the calibration period, verification period, and the entire period pass the significant level (Table 2), indicating that the $RH_{JA}$ exhibits high consistency with the instrumental data (Fritts 1976). Both the reduction of error (RE) and coefficient of efficiency (CE) are above zero, indicating robust and reliable reconstruction skills (Cook et al. 1999). In summary, the reconstructed model passed the split calibration-verification test, and the $RH_{JA}$ can be used to represent the local relative humidity from July to August. The $RH_{JA}$ is shown in Fig. 2d.

## Discussions

### Climatic response of $\delta^{18}O_{tree}$

The negative correlation between $\delta^{18}O_{tree}$ and the hydroclimatic index is explicable by the fractionation of tree-ring isotopes (McCarroll and Loader 2004). Constituent elements of tree-ring cellulose mainly come from $CO_2$, $H_2O$, and $O_2$, while $\delta^{18}O$ of tree-ring cellulose only depends on $H_2O$ (Deniro and Epstein 1979). $\delta^{18}O$ in the source water of trees varies with the isotopic signal of precipitation. The critical fractionation process of water is transpiration in leaves,

**Table 1** Statistical parameter of $\delta^{18}O_{tree}$ series and correlation coefficients among them

| | 01B | 03A | 16A | 17A | Composite |
|---|---|---|---|---|---|
| Statistical parameters | | | | | |
| Maximum value | 32.47‰ | 32.51‰ | 32.58‰ | 33.26‰ | 2.00 |
| Minimum value | 24.24‰ | 24.40‰ | 23.06‰ | 23.49‰ | − 2.74 |
| Mean value | 28.84‰ | 28.27‰ | 28.28‰ | 29.52‰ | 0.02 |
| First-order autocorrelation | 0.14 | 0.17 | 0.12 | 0.12 | 0.13 |
| Sequence time span | 1722–2013 | 1752–1997 | 1700–2013 | 1797–2013 | 1765–2013 |
| Standard deviation | 1.44‰ | 1.54‰ | 1.55‰ | 1.81‰ | 0.87 |
| Skewness | − 0.19 | − 0.05 | − 0.10 | − 0.42 | − 0.19 |
| Kurtosis | − 0.20 | − 0.30 | 0.12 | 0.39 | 0.06 |
| Correlation coefficients | | | | | |
| 03A | $r = 0.59$ | | | | |
| | 233/225 | | | | |
| 16A | $r = 0.66$ | $r = 0.58$ | | | |
| | 249/235 | 233/224 | | | |
| 17A | $r = 0.73$ | $r = 0.63$ | $r = 0.72$ | | |
| | 217/208 | 201/192 | 217/206 | | |
| Composite | $r = 0.87$ | $r = 0.82$ | $r = 0.87$ | $r = 0.90$ | |
| | 249/238 | 233/228 | 249/238 | 217/207 | |

($r$, N/EDOF) where EDOF is the effective degree of freedom; all $r$ values are significant at the 99.99% confidence level

where the sucrose forms by fixing the leaf water (McCarroll and Loader 2004). The intensity of transpiration is mainly influenced by relative humidity: a low relative humidity leads to strong transpiration, resulting in a high enrichment of $^{18}O$ in leaf water and it is vice versa for high relative humidity. During the formation of cellulose, the oxygen of sugars may be re-exchanged with source water in xylem, and the proportion of the exchanged oxygen atoms determines the proportion of relative humidity and $\delta^{18}O_{precipitation}$ signals in the cellulose (Anderson et al. 2002). The proportion is difficult to predict (Barbour and Farquhar 2000), but it can be seen from Fig. 2b that the correlation of $\delta^{18}O_{tree}$ and relative humidity is significant in this study.

The partial correlation coefficients of the $RH_{JA}$ with temperature and precipitation from July to August are − 0.15 (1961–2013, $p$ = 0.29) and 0.50 (1961–2013, $p$ < 0.001), respectively. Hence, the $RH_{JA}$ in this region is mainly related to the amount of precipitation. In addition, the precipitation is highest in July-August (Fig. 1b), and July-August can be regarded as the summer rainy season over North China. The seasonal advance of the EASM and the monsoon rainfall belt is stepwise rather than continuous (Ding and Chan 2005; Wu and Wang 2001). In late July, the monsoon rainfall belt jumps northward to North China from Meiyu/Baiu/Changma regions, and after a stationary period, it retreats back in mid-August (Wang and Lin 2002). Furthermore, the $RH_{JA}$ is significantly correlated with various monsoon indices (Table 3). There are various definitions of the monsoon index, which focus on various aspects of the monsoon circulation (Wang et al. 2008) due to the complexity of the East Asian monsoon

**Table 2** Statistics of the split calibration-verification

| Calibration | | | | Verification | | | | | |
|---|---|---|---|---|---|---|---|---|---|
| Period | $r$ | Sign test | $t$ | Period | $r$ | RE | CE | Sign test | $t$ |
| 1961–1986 | − 0.78** | 22+/4−** | 4.85** | 1987–2013 | − 0.57** | 0.52 | 0.27 | 19+/8−* | 5.48** |
| 1988–2013 | − 0.56** | 18+/8−* | 5.37** | 1961–1987 | − 0.80** | 0.74 | 0.58 | 22+/5−** | 5.00** |
| 1961–2013 | − 0.70** | 40+/13−** | 7.69** | | | | | | |

* Denotes the confidence level of 95%

** Denotes the confidence level of 99%

**Table 3** Correlation coefficients between $RH_{JA}$ and climate indices

| | r/EDOF | p | Period |
|---|---|---|---|
| EASMI(Shi and Zhu 1996) | − 0.34/53 | < 0.05 | 1948–2013 |
| EASMI(Lau et al. 2000) | 0.32/66 | < 0.01 | 1948–2013 |
| EASMI(Huang and Yan 1999) | 0.35/65 | < 0.005 | 1948–2013 |
| NINO1+2 | − 0.15/161 | < 0.1 | 1854–2013 |
| NINO3 | − 0.21/164 | < 0.01 | 1854–2013 |
| NINO3.4 | − 0.26/159 | < 0.001 | 1854–2013 |
| NINO4 | − 0.33/150 | < 0.001 | 1854–2013 |
| SOI | 0.19/131 | < 0.05 | 1882–2013 |
| MEI | − 0.42/64 | < 0.001 | 1950–2013 |

system. As a result, the $RH_{JA}$ is mainly influenced by precipitation in the summer rainy season and further by the EASM.

## Spatial representation of $RH_{JA}$

A spatial correlation analysis of the instrumental calibration period (Fig. 1a) and reconstructed period (Fig. 3b) shows a significant positive correlation with the dry/wet variations in most parts of North China around the sampling point. The $RH_{JA}$ was significantly correlated with other proxy series near the sampling site in previous studies (Fig. 3a). However, the dryness/wetness index (DWI-37) has a significant correlation with the $RH_{JA}$ at high frequency but not at low frequency, which may be because historical documents are difficult to capture the interdecadal trend in climate change. Therefore, to represent the climate situation more accurately, the characteristics of the selected proxy data (Schneider et al. 2019) should be taken into account when investigating past climate change. All in all, the $RH_{JA}$ can represent the dry/wet variations in a large area covering most parts of North China.

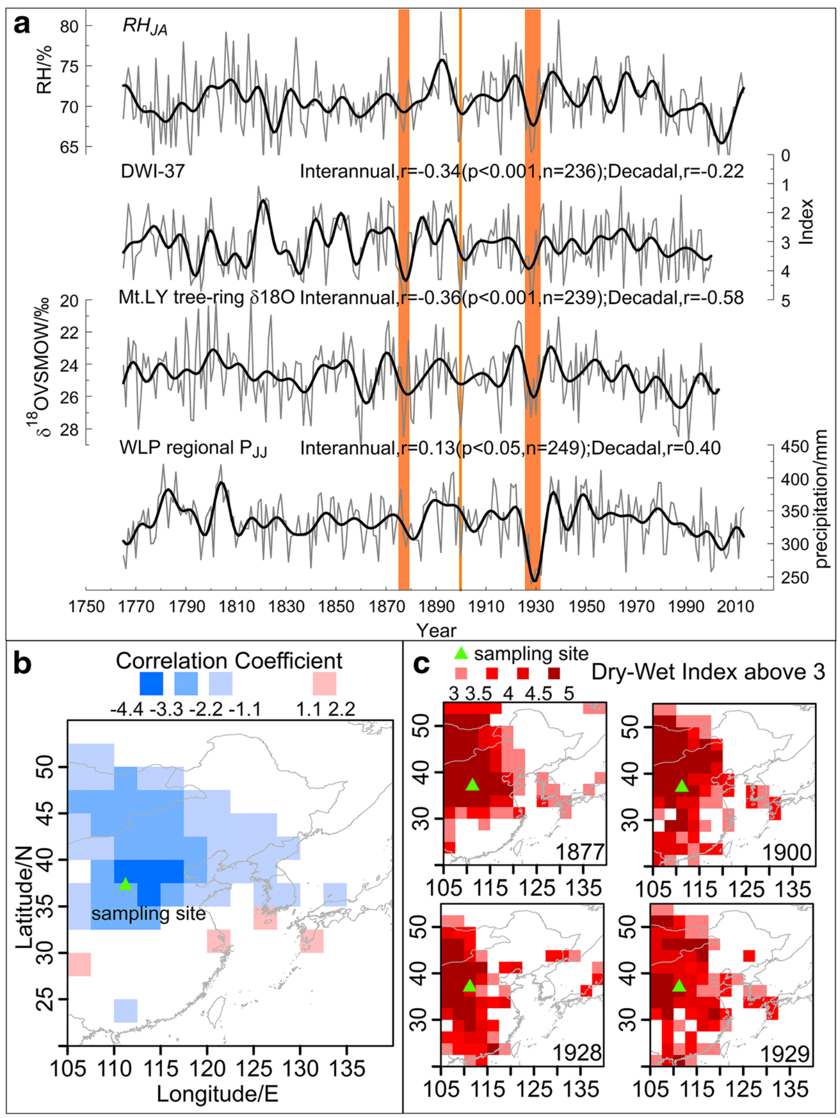


**Fig. 3** **a** $RH_{JA}$ and other proxy series near the sampling point in previous studies: DWI-37 (38.75° N, 111.25° E) is the nearest point to the sampling site in the Yang et al. (2013) dataset; Mt.LY is the tree-ring $\delta^{18}O$ data from Mt. Luya (38° 44′ N,111° 50′ E), where a smaller $\delta^{18}O$ value represents wetter conditions and vice versa (Li et al. 2011); WLP is the regional precipitation series from previous-year July to current-year June reconstructed from 10 tree-ring width chronologies in the Loess Plateau Region (33.8° N–40.5° N,100° E–107° E) of the central-western edge of the Asian summer monsoon (Liu et al. 2019). The related coefficients of $RH_{JA}$ with other proxy series are marked in the figure. **b** Spatial correlation analysis of the $RH_{JA}$ using the gridded DWI dataset from 1765 to 2013 AD, only coloring the significant correlation region ($p < 10\%$). **c** Drought (DWI > 3) distribution in four extensive drought years (1877, 1900, 1928, and 1929 AD). All grid values are based on the DWI, denoting drought, and flood as 1-very wet, 2-wet, 3-normal, 4-dry, and 5-very dry (Yang et al. 2013)

## Extensive drought events and the ENSO impact on $RH_{JA}$

The mean value of the relative humidity reconstruction sequence is 70.71%, and the standard deviation is 3.45%. From an interannual perspective, we defined extremely wet years as having a relative humidity higher than 74.16% (mean + $\alpha$) and extremely dry years as having a relative humidity below 67.26% (mean − $\alpha$). In the reconstructed 249 years, extremely wet and dry years accounted for 14.46% (36 years) and 16.47% (41 years), respectively (Table 4). According to Table 4, the $RH_{JA}$ recorded many widely reported serious drought events, such as the Dingwu Extraordinary Drought from 1876 to 1878 (Cook et al. 2010; Zhang and Liang 2010; Hao et al. 2010), drought in the 1900 (Dong et al. 2015) and 1920s drought from 1922 to 1932(Liang et al. 2006). The droughts in 1877, 1900, and 1928–1929 are widely distributed, demonstrating by the DWI gridded dataset (Fig. 3c) and other proxy records (Fig. 3a), suggesting that they are extensive drought events.

It is noteworthy that the extreme dry/wet years always co-occurred with ENSO events (Table 4). A correlation analysis shows that $RH_{JA}$ is significantly correlated with different ENSO indices (Table 3). In addition, a multi-taper method

**Table 4** Extreme dry/wet years and relevant ENSO events*

| Rank | Year | Wet (%) | La Niña event | Rank | Year | Dry (%) | El Niño event |
|---|---|---|---|---|---|---|---|
| 1 | 1892 | 81.68 | Strong | 1 | 1777 | 62.86 | Weak |
| 2 | 1939 | 80.70 | P4-C4 | 2 | 2007 | 63.05 | *P7-C2* |
| 3 | 1806 | 79.16 | | 3 | 1827 | 63.17 | |
| 4 | 1815 | 78.94 | | 4 | 1792 | 63.21 | Weak |
| 5 | 1834 | 78.51 | | 5 | 1821 | 63.38 | |
| 6 | 1809 | 78.07 | Strong | 6 | 1916 | 63.53 | *P1-P8* |
| 7 | 1789 | 77.94 | | 7 | 2003 | 63.91 | *P8-C4* |
| 8 | 1922 | 77.89 | *P3-P7* | 8 | 1928 | 64.30 | |
| 9 | 1924 | 76.94 | C5-N3 | 9 | 1929 | 64.81 | |
| 10 | 1894 | 76.47 | Extreme | 10 | 1784 | 64.90 | Weak |
| 11 | 1893 | 76.43 | Very Strong | 11 | 1824 | 64.92 | Moderate |
| 12 | 1981 | 76.42 | *P1-P6* | 12 | 1786 | 65.04 | |
| 13 | 1917 | 76.32 | P2-N4 | 13 | 1999 | 65.04 | *P1-P6* |
| 14 | 1967 | 76.20 | C5-C8 | 14 | 1782 | 65.29 | Weak |
| 15 | 1954 | 76.10 | C7-N12 | 15 | 1780 | 65.38 | |
| 16 | 1801 | 76.07 | Very Strong | 16 | 2005 | 65.39 | |
| 17 | 1966 | 76.02 | N5-N8 | 17 | 1899 | 65.60 | C8-N8 |
| 18 | 1871 | 76.00 | Very Strong | 18 | 1846 | 65.66 | Weak |
| 19 | 1778 | 75.91 | Weak | 19 | 1791 | 65.75 | Very Strong |
| 20 | 1919 | 75.71 | | 20 | 1869 | 65.93 | |
| 21 | 1818 | 75.66 | | 21 | 1838 | 66.15 | Weak |
| 22 | 1794 | 75.58 | | 22 | 1832 | 66.33 | Weak |
| 23 | 1842 | 75.57 | | 23 | 1982 | 66.34 | C4-N9 |
| 24 | 1807 | 75.50 | | 24 | 1813 | 66.35 | |
| 25 | 1964 | 75.33 | C4-C12 | 25 | 1795 | 66.35 | |
| 26 | 1935 | 75.29 | | 26 | 2002 | 66.36 | C9-N4 |
| 27 | 1937 | 75.27 | *N3-N12* | 27 | 2001 | 66.39 | |
| 28 | 1940 | 75.13 | *P1-P5* | 28 | 1900 | 66.40 | Very Strong |
| 29 | 1811 | 75.09 | | 29 | 1987 | 66.41 | P8-N3 |
| 30 | 1975 | 74.96 | C3-N6 | 30 | 2008 | 66.46 | *N6-N12* |
| 31 | 1771 | 74.94 | | 31 | 1828 | 66.59 | |
| 32 | 1767 | 74.72 | | 32 | 1992 | 66.66 | P10-C9 |
| 33 | 1931 | 74.58 | | 33 | 1980 | 66.68 | P2-C6 |
| 34 | 1909 | 74.30 | P3-C6 | 34 | 1936 | 66.73 | |
| 35 | 1912 | 74.22 | *P1-P8* | 35 | 2006 | 66.73 | C7-N2 |
| 36 | 1800 | 74.19 | | 36 | 1877 | 66.78 | Very Strong |
| | | | | 37 | 1860 | 66.81 | Weak |
| | | | | 38 | 1804 | 66.82 | Weak |
| | | | | 39 | 1965 | 66.83 | C6-N5 |
| | | | | 40 | 1926 | 67.05 | P8-C6 |
| | | | | 41 | 1881 | 67.09 | Moderate |

* The ENSO events in 1985–2013 AD refer to the top 24 strongest El Niño and La Niña event years by season (https://psl.noaa.gov/enso/past_events.html) determined using PSL's Extended Multivariate ENSO. The months are marked numerically in the table, where P, C, and N denote the previous year, current year, and next year. The italics indicate weak relevance when July and August are not included in the ENSO months. The ENSO events in 1765–1894 AD refer to the annual record of ENSO events (Gergis and Fowler 2009), and the intensity is marked in the table

(MTM) spectral analysis (Fig. 2f) shows that the $RH_{JA}$ has 2.1–4.2 high-frequency quasi-cycles, which agrees with the quasi-cycle (2–7 years) of the ENSO. To conclude, ENSO plays an important role in the interannual variations of $RH_{JA}$ in North China. In fact, El Niño events always lead to negative precipitation anomalies in North China. It is mainly because the western Pacific subtropical high (WPSH) strengthening and shifting westward, and the weakening of Indian summer monsoon induces moisture inflow to North China (Zhang et al. 1999). The situation is vice versa for La Niña events.

### The unprecedented weakening of the Asian summer monsoon since the late 1970s

Regarding the 11-year moving average of the $RH_{JA}$, there is a significant drying trend after the 1970s (Fig. 1c). Four main transition points were detected using a sliding $t$ test and Mann-Kendall test (Mann 1945), dividing the $RH_{JA}$ into 5 periods (Fig. 2d). The period of 1981–2013 represents an unprecedented drought period throughout the past two and a half centuries. Considering the significant correlation between $RH_{JA}$ and EASM, it can be inferred that the weakening of the EASM since the late 1970s was unprecedented in the past two and a half centuries. In fact, during the middle and late 1970s, abrupt changes in precipitation occurred in the East Asian monsoon region (Ding et al. 2008), which is related to the weakening of the EASM circulation after the end of the 1970s (Wang 2001). The leading factor for the weakening of the EASM since the late 1970s is the recent warming of the tropical ocean centered over the central and eastern Pacific Ocean (Zeng et al. 2007; Li et al. 2010).

In addition, it has been widely reported that the weakening of the EASM since the late 1970s has resulted in a "southern China flood and northern China drought" bipolar rainfall pattern in the monsoon region of China (Ding et al. 2008; Zhou et al. 2009a). A significant negative correlating pattern is present in the lower reaches of the Yangtze River Basin, southern Japan and southern Korea, according to the spatial correlation analysis results using the gridded rainfall dataset (Fig. 1a). The regional land rainfall sequence in this region (30° –37° N,115°–131° E) shows an increasing trend and a significantly negative correlation with $RH_{JA}$ after 1965 (Fig. 1c). This region corresponds to the Meiyu/Baiu/Changma rainfall belt, and the rainfall in this region has increased since the late 1970s (Ho et al. 2003). Following the warming of the tropical Pacific Ocean, the WPSH (one important component of the ESAM) has extended westward since the late 1970s (Zhou et al. 2009b), increasing summer rainfall over the Yangtze River valley (Chang et al. 2000; Gong and Ho 2002).

Moreover, the $RH_{JA}$ shows a significant correlation with the dry/wet variations across India in the spatial correlation analysis (Fig. 1a). This finding can be explained by the teleconnection between rainfall across India and North China, which has been widely reported for the instrumental period (Hu et al. 2005; Wu 2017). Similar to the ESAM, the Indian summer monsoon circulation has also weakened since the late 1970s along with recent warming of the tropical ocean (Wu 2005; Lin et al. 2017).

## Conclusions

The tree-ring $\delta^{18}O$ of Chinese pine from Mt. Beiwudang mainly reflects the relative humidity signal of July to August. The relative humidity of July and August from 1765 to 2013 was reconstructed using a linear regression model, and the reconstructed $RH_{JA}$ explains 49% of the instrumental variance during the period of 1961–2013. The $RH_{JA}$ can represent the dry/wet variations of the summer rainy season in a large area covering most parts of North China to some extent. There were 41 (36) extremely dry (wet) years over the past two and a half centuries and the extreme dry/wet years always co-occurred with ENSO events. In addition to the significant correlation coefficient between $RH_{JA}$ and ENSO index and the similar quasi-cycle with ENSO, it can be inferred that ENSO played an important role in the interannual variations of $RH_{JA}$ in North China. Based on the good relationship between the $RH_{JA}$ and EASM, the $RH_{JA}$ captures the recent weakening of the EASM since the late 1970s and suggests the recent weakening is unprecedented in the past two and a half centuries. At the same time, the precipitation over the Meiyu/Baiu/Changma rainfall belt region has increased and the precipitation over India has decreased due to the recent warming of the tropical ocean according to previous papers.

In general, the tree-ring cellulose $\delta^{18}O$ data show a strong advantage in paleoclimatic reconstruction. However, single-site research is insufficient to testify to the regional interrelation and reflect climate change over the entire Asian summer monsoon (ASM) system, but it can be a clue to further regional research. It is meaningful to build a proxy network reflecting more detail of the interannual to interdecadal ASM climatic changes and even global changes.

**Funding** This study was jointly supported by grants from the Strategic Priority Research Program of the Chinese Academy of Sciences (CAS) (XDB40000000), the National Natural Science Foundation of China (41630531), the Chinese Academy of Sciences (QYZDJ–SSW–DQC021, XDA23070202, 2019QZKK0101, and GJHZ1777), the State Key Laboratory of Loess and Quaternary Geology, Institute of Earth Environment, CAS (SKLLQG1804) and other grants from the IEECAS and the SKLLQG.

**Data availability** Not applicable

### Compliance with ethical standards

**Conflict of interest** The authors declare that they have no conflict of interest.

**Code availability** Not applicable

## References


An ZS, Porter SC, Kutzbach JE et al (2000) Asynchronous Holocene optimum of the East Asian monsoon. Quaternary Sci Rev 19:743–762. https://doi.org/10.1016/s0277-3791(99)00031-1

Anderson WT, Bernasconi SM, McKenzie JA et al (2002) Model evaluation for reconstructing the oxygen isotopic composition in precipitation from tree ring cellulose over the last century. Chem Geol 182:121–137. https://doi.org/10.1016/s0009-2541(01)00285-6

Baker PJ, Palmer JG, D'Arrigo R (2008) The dendrochronology of Callitris intratropica in northern Australia: annual ring structure, chronology development and climate correlations. Aust J Bot 56:311–320. https://doi.org/10.1071/bt08040

Barbour MM, Farquhar GD (2000) Relative humidity- and ABA-induced variation in carbon and oxygen isotope ratios of cotton leaves. Plant Cell Environ 23:473–485. https://doi.org/10.1046/j.1365-3040.2000.00575.x

Briffa KR, Osborn TJ, Schweingruber FH, Harris IC, Jones PD, Shiyatov SG, Vaganov EA (2001) Low-frequency temperature variations from a northern tree ring density network. J Geophys Res-Atmos 106:2929–2941. https://doi.org/10.1029/2000jd900617

Cai QF, Liu Y, Bao GA, Lei Y, Sun B (2010) Tree-ring-based May-July mean temperature history for Luliang Mountains, China, since 1836. Chinese Sci Bull 55:3008–3014. https://doi.org/10.1007/s11434-010-3235-z

Chang CP, Zhang YS, Li T (2000) Interannual and interdecadal variations of the East Asian summer monsoon and tropical Pacific SSTs. Part I: Roles of the subtropical ridge. J Climate 13:4310–4325. https://doi.org/10.1175/1520-0442(2000)013<4310:iaivot>2.0.co;2

Chen F, Yuan Y, Wei W, Yu S, Wang H (2015) Tree-ring response of subtropical tree species in southeast China on regional climate and sea-surface temperature variations. Trees-Struct Funct 29:17–24. https://doi.org/10.1007/s00468-013-0951-4

Cook ER, Anchukaitis KJ, Buckley BM, D'Arrigo RD, Jacoby GC, Wright WE (2010) Asian monsoon failure and megadrought during the last millennium. Science 328:486–489. https://doi.org/10.1126/science.1185188

Cook ER, Meko DM, Stahle DW, Cleaveland MK (1999) Drought reconstructions for the continental United States. J Climate 12:1145–1162. https://doi.org/10.1175/1520-0442(1999)012<1145:drftcu>2.0.co;2

Coplen TB, Brand WA, Gehre M, Gröning M, Meijer HAJ, Toman B, Verkouteren RM (2006) New guidelines for delta C-13 measurements. Anal Chem 78:2439–2441. https://doi.org/10.1021/ac052027c

Deniro MJ, Epstein S (1979) Relationship between the oxygen isotope ratios of terrestrial plant cellulose, carbon-dioxide, and water. Science 204:51–53. https://doi.org/10.1126/science.204.4388.51

Ding YH, Chan JCL (2005) The East Asian summer monsoon: an overview. Meteorol Atmos Phys 89:117–142. https://doi.org/10.1007/s00703-005-0125-z

Ding Y, Wang Z, Sun Y (2008) Inter-decadal variation of the summer precipitation in East China and its association with decreasing Asian summer monsoon. Part I: Observed evidences. Int J Climatol 28:1139–1161. https://doi.org/10.1002/joc.1615

Dong A, Li Y, Zhang Y (2015) Characteristics and formative natural factors of extreme drought in china around 1900. Plateau Meteorology 34:771-776(In Chinese)

Durbin J, Watson GS (1950) Testing for serial correlation in least squares regression. 1. Biometrika 37:409–428. https://doi.org/10.2307/2332391

Fonti P, von Arx G, Garcia-Gonzalez I et al (2010) Studying global change through investigation of the plastic responses of xylem anatomy in tree rings. New Phytol 185:42–53. https://doi.org/10.1111/j.1469-8137.2009.03030.x

Fowler A, Boswijk G, Ogden J (2004) Tree-ring studies on Agathis australis (kauri): a synthesis of development work on Late Holocene chronologies. Tree-Ring Res 60:15–29. https://doi.org/10.3959/1536-1098-60.1.15

Fritts HC (1976) Tree Rings and Climate. Academic Press, New York

Fritts HC (1991) Reconstructing large-scale climatic patterns from tree-ring data: a diagnostic analysis. The University of Arizona Press, Tucson

Gergis JL, Fowler AM (2009) A history of ENSO events since AD 1525: implications for future climate change. Climatic Change 92:343–387. https://doi.org/10.1007/s10584-008-9476-z

Gong DY, Ho CH (2002) Shift in the summer rainfall over the Yangtze River valley in the late 1970s. Geophys Res Lett 29:78-1–78-4. https://doi.org/10.1029/2001gl014523

Hao Z, Zheng J, Wu G, Zhang XZ, Ge QS (2010) 1876-1878 severe drought in North China: facts, impacts and climatic background. Chinese Sci Bull 55:3001–3007. https://doi.org/10.1007/s11434-010-3243-z

Ho CH, Lee JY, Ahn MH, Lee HS (2003) A sudden change in summer rainfall characteristics in Korea during the late 1970s. Int J Climatol 23:117–128. https://doi.org/10.1002/joc.864

Holmes RL (1983) Computer-assisted quality control in tree-ring dating and measurement. Tree-ring Bull 43:69–78

Hu ZZ, Wu RG, Kinter JL, Yang S (2005) Connection of summer rainfall variations in South and East Asia: Role of El Nino-southern oscillation. Int J Climatol 25:1279–1289. https://doi.org/10.1002/joc.1159

Huang G, Yan ZW (1999) The East Asian summer monsoon circulation anomaly index and its interannual variations. Chinese Sci Bull 44:1325–1329. https://doi.org/10.1007/bf02885855

Lau KM, Kim KM, Yang S (2000) Dynamical and boundary forcing characteristics of regional components of the Asian summer monsoon. J Climate 13:2461–2482. https://doi.org/10.1175/1520-0442(2000)013<2461:dabfco>2.0.co;2

Leavitt SW (2010) Tree-ring C-H-O isotope variability and sampling. Sci Total Environ 408:5244–5253. https://doi.org/10.1016/j.scitotenv.2010.07.057

Li H, Dai A, Zhou T, Lu J (2010) Responses of East Asian summer monsoon to historical SST and atmospheric forcing during 1950-2000. Clim Dynam 34:501–514. https://doi.org/10.1007/s00382-008-0482-7

Li Q, Nakatsuka T, Kawamura K, Liu Y, Song H (2011) Hydroclimate variability in the North China Plain and its link with El Nino-Southern Oscillation since 1784 AD: Insights from tree-ring cellulose delta O-18. J Geophys Res-Atmos 116. https://doi.org/10.1029/2011jd015987

Liang E, Liu X, Yuan Y, Qin N, Fang X, Huang L, Zhu H, Wang L, Shao X (2006) The 1920S drought recorded by tree rings and historical documents in the semi-arid and arid areas of Northern China. Climatic Change 79:403–432. https://doi.org/10.1007/s10584-006-9082-x

Lin Z, Lu R, Wu R (2017) Weakened impact of the Indian early summer monsoon on north china rainfall around the late 1970s: role of basic-state change. J Climate 30:7991–8005. https://doi.org/10.1175/jcli-d-17-0036.1

Liu Y, Cai W, Sun C, Song H, Cobb KM, Li J, Leavitt SW, Wu L, Cai Q, Liu R, Ng B, Cherubini P, Büntgen U, Song Y, Wang G, Lei Y, Yan L, Li Q, Ma Y, Fang C, Sun J, Li X, Chen D, Linderholm HW (2019) Anthropogenic Aerosols cause recent pronounced weakening of Asian summer monsoon relative to last four centuries. Geophys Res Lett 46:5469–5479. https://doi.org/10.1029/2019gl082497

Liu Y, Ren M, Li Q et al (2020) Tree-ring delta O-18-based July-August relative humidity reconstruction on Mt. Shimen, China, for the last 400 years. Atmos Res 243. https://doi.org/10.1016/j.atmosres.2020.105024

Liu Y, Wang RY, Leavitt SW, Song HM, Linderholm HW, Li Q, An Z (2012) Individual and pooled tree-ring stable-carbon isotope series in Chinese pine from the Nan Wutai region, China: common signal and climate relationships. Chem Geol 330:17–26. https://doi.org/10.1016/j.chemgeo.2012.08.008

Ljungqvist FC, Krusic PJ, Sundqvist HS et al (2016) Northern Hemisphere hydroclimate variability over the past twelve centuries. Nature 532:94-+. https://doi.org/10.1038/nature17418

Loader NJ, Robertson I, Barker AC, Switsur VR, Waterhouse JS (1997) An improved technique for the batch processing of small wholewood samples to alpha-cellulose. Chem Geol 136:313–317. https://doi.org/10.1016/s0009-2541(96)00133-7

Mann HB (1945) NONPARAMETRIC TESTS AGAINST TREND. Econometrica 13:245–259. https://doi.org/10.2307/1907187

Mann ME, Zhang Z, Rutherford S, Bradley RS, Hughes MK, Shindell D, Ammann C, Faluvegi G, Ni F (2009) Global Signatures and Dynamical Origins of the Little Ice Age and Medieval Climate Anomaly. Science 326:1256–1260. https://doi.org/10.1126/science.1177303

McCarroll D, Loader NJ (2004) Stable isotopes in tree rings. Quaternary Sci Rev 23:771–801. https://doi.org/10.1016/j.quascirev.2003.06.017

Pearl JK, Keck JR, Tintor W, Siekacz L, Herrick HM, Meko MD, Pearson CL (2020) New frontiers in tree-ring research. Holocene 30:923–941. https://doi.org/10.1177/0959683620902230

Schneider L, Ljungqvist FC, Yang B, Chen F, Chen J, Li J, Hao Z, Ge Q, Talento S, Osborn TJ, Luterbacher J (2019) The impact of proxy selection strategies on a millennium-long ensemble of hydroclimatic records in Monsoon Asia. Quaternary Sci Rev 223:105917. https://doi.org/10.1016/j.quascirev.2019.105917

Shi N, Zhu QG (1996) An abrupt change in the intensity of the East Asian summer monsoon index and its relationship with temperature and precipitation over east China. Int J Climatol 16:757–764. https://doi.org/10.1002/(sici)1097-0088(199607)16:7<757::aid-joc50>3.0.co;2-5

Wang HJ (2001) The weakening of the Asian monsoon circulation after the end of 1970's. Adv Atmos Sci 18:376–386. https://doi.org/10.1007/BF02919316

Wang B, Lin HO (2002) Rainy season of the Asian-Pacific summer monsoon. J Climate 15:386–398. https://doi.org/10.1175/1520-0442(2002)015<0386:rsotap>2.0.co;2

Wang B, Wu ZW, Li JP, Liu J, Chang CP, Ding Y, Wu G (2008) How to measure the strength of the East Asian summer monsoon. J Climate 21:4449–4463. https://doi.org/10.1175/2008jcli2183.1

Wigley TML, Briffa KR, Jones PD (1984) On the average value of correlated time-series, with applications in dendroclimatology and hydrometeorology. J Clim Appl Meteor 23:201–213. https://doi.org/10.1175/1520-0450(1984)023<0201:Otavoc>2.0.Co;2

Wu BY (2005) Weakening of Indian summer monsoon in recent decades. Adv Atmos Sci 22:21–29. https://doi.org/10.1007/BF02930866

Wu R (2017) Relationship between Indian and East Asian summer rainfall variations. Adv Atmos Sci 34:4–15. https://doi.org/10.1007/s00376-016-6216-6

Wu R, Wang B (2001) Multi-stage onset of the summer monsoon over the western North Pacific. Clim Dynam 17:277–289. https://doi.org/10.1007/s003820000118

Yang B, Qin C, Wang J, He M, Melvin TM, Osborn TJ, Briffa KR (2014) A 3,500-year tree-ring record of annual precipitation on the northeastern Tibetan Plateau. P Natl Acad Sci USA 111:2903–2908. https://doi.org/10.1073/pnas.1319238111

Yang FM, Shi F, Kang SY, Wang S, Xiao Z, Nakatsuka T, Shi J (2013) Comparison of the dryness/wetness index in China with the Monsoon Asia Drought Atlas. Theor Appl Climatol 114:553–566. https://doi.org/10.1007/s00704-013-0858-4

Zeng G, Sun Z, Wang W-C, Min J (2007) Interdecadal variability of the east Asian summer monsoon and associated atmospheric circulations. Adv Atmos Sci 24:915–926. https://doi.org/10.1007/s00376-007-0915-y

Zhang D, Liang Y (2010) A long lasting and extensive drought event over China in 1876-1878. Adv Clim Chang Res 6:106–112. https://doi.org/10.3724/SP.J.1248.2010.00091

Zhang RH, Sumi A, Kimoto M (1999) A diagnostic study of the impact of El Nino on the precipitation in China. Adv Atmos Sci 16:229–241. https://doi.org/10.1007/bf02973084

Zhou T, Gong D, Li J, Li B (2009a) Detecting and understanding the multi-decadal variability of the East Asian Summer Monsoon - recent progress and state of affairs. Meteorol Z 18:455–467. https://doi.org/10.1127/0941-2948/2009/0396

Zhou T, Yu R, Zhang J, Drange H, Cassou C, Deser C, Hodson DLR, Sanchez-Gomez E, Li J, Keenlyside N, Xin X, Okumura Y (2009b) Why the Western Pacific subtropical high has extended westward since the late 1970s. J Climate 22:2199–2215. https://doi.org/10.1175/2008jcli2527.1